Supporting Information

Shipping Remains a Globally Significant Source of Anthropogenic PN Emissions Even after 2020 Sulfur Regulation

Niina Kuittinen[a], Jukka-Pekka Jalkanen[b], Jenni Alanen[a], Leonidas Ntziachristos[a], Hanna Hannuniemi[b], Lasse Johansson[b], Panu Karjalainen[a], Erkka Saukko[a], Mia Isotalo[a], Päivi Aakko-Saksa[c], Kati Lehtoranta[c], Jorma Keskinen[a], Pauli Simonen[a], Sanna Saarikoski[b], Eija Asmi[b], Tuomas Laurila[b], Risto Hillamo[b], Fanni Mylläri[a], Heikki Lihavainen[b,d], Hilkka Timonen[b], Topi Rönkkö[a]

[a]Aerosol Physics Laboratory, Physics Unit, Faculty of Engineering and Natural Sciences, Tampere University, FI-33014, Tampere, Finland

[b]Atmospheric Composition Research, Finnish Meteorological Institute, P.O. Box 503, 00101 Helsinki, Finland

[c]VTT Technical Research Centre of Finland Ltd., P.O. Box 1000, 02044 VTT, Espoo, Finland

[d]Svalbard Integrated Arctic Earth Observing System, P.O. Box 156, 9171 Longyearbyen, Norway

Number of pages: 16

Number of figures: 10

Number of tables: 7

Contents:

Supporting Information Text

Applying condensation particle counters with varying cut-points. In this work, CPCs with different cut-points were applied in different phases of the study. In the first laboratory campaign and on-board study, a CPC with 7nm cut-point was applied. In the second laboratory study, it was expected that the particles resulted from the combustion of natural gas could appear in very small size range and an ultrafine CPC with 3nm cut-point was chosen. In the plume chase studies, either a CPC with 3nm or 10 nm cut-point was available. The effect of using a CPC with a cut-point of 10nm or 7nm compared to the CPC with 3nm cut-point can be estimated based on the particle number size distributions for different fuels presented in this study (Figure 1A and 1B). For the EF_{PN} presented in Figure 1C and applied to STEAM, the error introduced by using a CPC with 7nm cut-point compared to one with 3nm cut-point in the cases of HFO, IFO and BIO30 is negligible, with less than 0.05% of particles being uncounted due to the higher cut-point. In the plume chase measurements, all the ships whose fuel information could be obtained burned either HFO or IFO, and it is assumed that the error introduced by the 10nm cut-point in part of the measurements is also small, between 0.05 and 0.3%. However, if LNG ships would have been chased, the influence could have been more significant, up to 4%.

Calculating the plume age. During the Skyvan flights, the maximum in-plume flight duration, on which continuous size distribution spectra, particle number concentration data, and gas component concentrations could be obtained, was 120 s. As the velocity of the aircraft was much higher than the prevailing wind and ship velocities, an effective aging of the plume of up to 600 s was captured. The proper age of the exhaust during Skyvan measurements was calculated from the velocities of the ship, aircraft and the prevailing wind. The time correction from the sampling

timeframe to the real atmospheric ageing timeframe has been calculated analogously to general Doppler Effect (1) (see Supporting Information and Figure S7)

$$\gamma = ||V_a - W|| / ||V_s - W|| \quad (1)$$

where V_a, W, and V_s denote the aircraft, wind and ship velocity vectors along the plume direction, respectively, with the V_a required to be for an in-plume flight. The wind speed and direction were obtained as an average of three nearby weather stations at Helsinki (Helsingin majakka), Porvoo (Kalbådagrund) and Kirkkonummi Mäkiluoto. The corresponding wind data was then calculated at the aircraft flight height using the power-law wind velocity profile method (2) and an assumption of neutral atmospheric conditions.

The age of the ship plume when it crosses the sampling inlet in the aircraft can be resolved analogous to Doppler phenomenon in the general case with a moving source and a moving observer. In the most simple case with wind speed (W) zero, the ageing factor would naturally be the ratio of aircraft speed (V_a) and ship speed (V_s). In the most complex case with different wind, aircraft and ship speed directions, the angles between the three need to be taken into account (see Figure S7). In a frame of reference moving with air, the plume length emitted in time $\Delta\tau$ can be expressed as $\Delta Ss = \Delta\tau(W\text{-}V_s)$ and plume length captured by the aircraft as $\Delta S_a = \Delta\tau(W\text{-}V_a)$. Therefore, time dilation, i.e. the time correction γ from the sampling timeframe to the real atmospheric ageing timeframe can be given as

$$\gamma = |\Delta\mathbf{S_a}|/ |\Delta\mathbf{S_s}| = |(\mathbf{V_a}\text{-}\mathbf{W})|/ |(\mathbf{V_s}\text{-}\mathbf{W})|.$$

The situation is analogous to Doppler formula in the general case. See the example of Neipp et al. (1), equation (8). The time correction from the sampling timeframe to the real atmospheric ageing timeframe is defined as the age of the emission divided by time measured. Thus,

$\gamma = 1/\omega \,/\, 1/\omega' = \omega'/\omega = (c\text{-}v_O)\cdot\mathbf{n}/(c\text{-}v_O)\cdot\mathbf{n}$.

Because here the aircraft was flying in the plume, $\gamma = |(\mathbf{v}_O\text{-}\mathbf{c})|/|(\mathbf{v}_S\text{-}\mathbf{c})|$. If we denote $c = \mathbf{W}$, $v_O = \mathbf{V}_a$, and $v_S = \mathbf{V}_s$ it follows that $\gamma = |(\mathbf{V_a}\text{-}\mathbf{W})|/|(\mathbf{V_s}\text{-}\mathbf{W})|$.

In calculating the plume age, flight height was considered only in the wind speed profile. However, the time it takes for the plume to rise to the flying height was not accounted for, and thus, the actual ageing times of the plumes may be longer than the calculated values. Other sources of uncertainty are the wind speeds and directions; the wind velocity at the measurement location was assumed to be the same as the one at the nearest weather station corrected with the power-law wind velocity profile method for the height difference of the weather station and the aircraft. In addition, the ship trajectory was assumed straight.

Inclusion of scrubbers in STEAM model. For the base year 2016, scrubber installations were found in 210 vessels and the installation dates and equipment types (closed/open loop, hybrid) were included in STEAM and obtained from shipyard reference lists, equipment manufacturers, and ship owner fleet descriptions. According to classification society guidance, 3% increase in power and fuel consumption due to pumps and coolers was implemented for vessels using open-loop scrubbers (3). While accounting for added power consumption due to scrubbers, in the run for 2016, we did not include the effect of scrubber on EF_{PN}, since only about 0.2% of the fleet (1.4% of global fuel consumption) was equipped with scrubber, and the impact of this assumption was expected to be negligible. The scrubber reduction efficiency was determined from on-board measurements. Due to the fairly low sulfur level of the HFO burned by the ship (0.7%S), the scrubber reduction efficiency was applied to the EF_{PN} for 2.2%S HFO and this was used in the global scenario calculations to represent ships equipped with scrubbers burning HFO.

References

1. C. Neipp *et al.* An analysis of the classical Doppler effect. *Eur. J. Phys.* **24**, 407–505 (2003).

2. J. H. Seinfeld and S. N. Pandis. *Atmospheric Chemistry and Physics: From Air Pollution to Climate Change.* (John Wiley & Sons, Hoboken, ed. 3, 2016) p. 700.

3. "Exhaust Gas Scrubber Systems" (American Bureau of Shipping, 2018); https://ww2.eagle.org/content/dam/eagle/advisories-and-debriefs/exhaust-gas-scrubber-systems-advisory.pdf

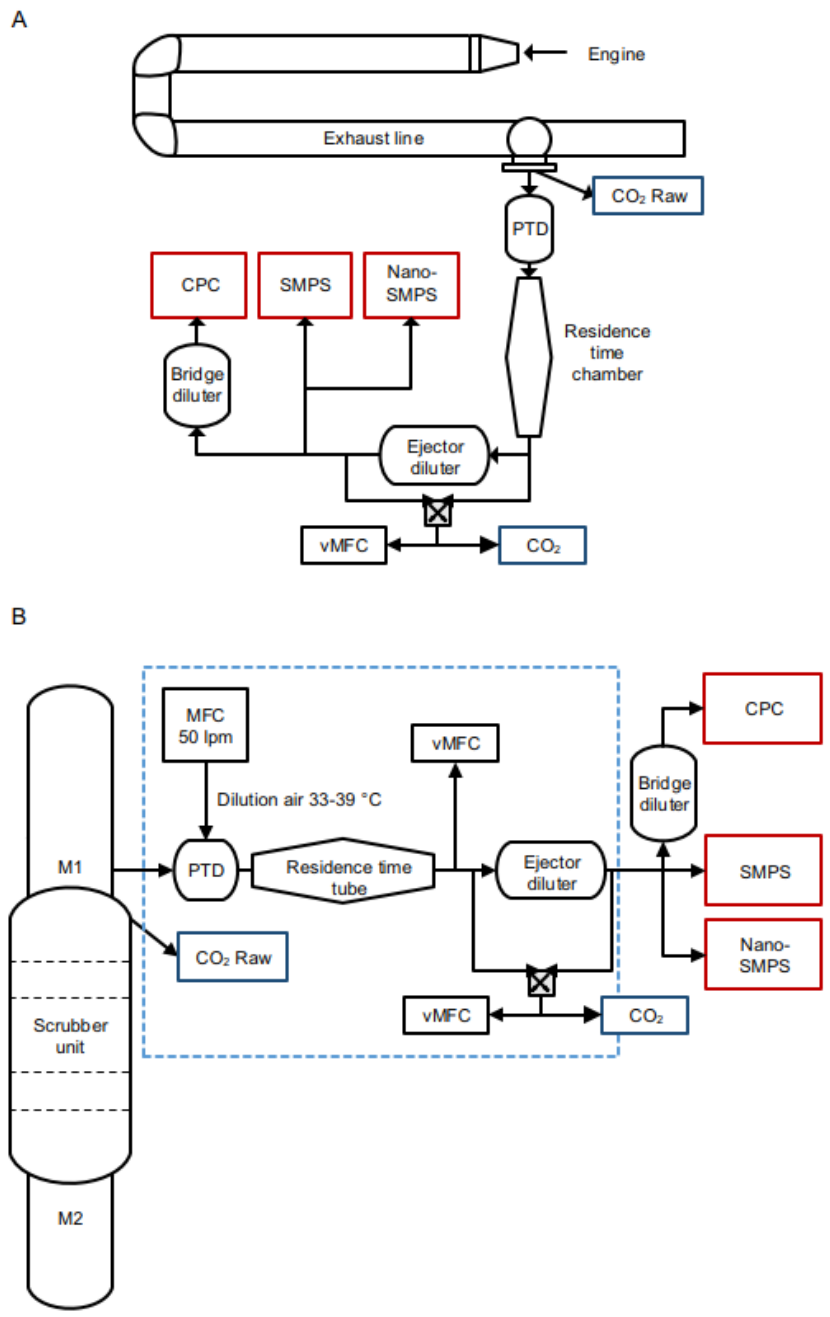

Figure S1. Dilution and positioning of devices in laboratory and on-board measurements. A. Measurement setup during of test-bench measurements. Exhaust was sampled from 5.9 m downstream of the turbo charger. B. Measurement devices and sampling locations during on-board testing where exhaust was sampled right before and after the scrubber. M1 marks sampling location in the exhaust tunnel after scrubber and M2 sampling location right before the scrubber unit.

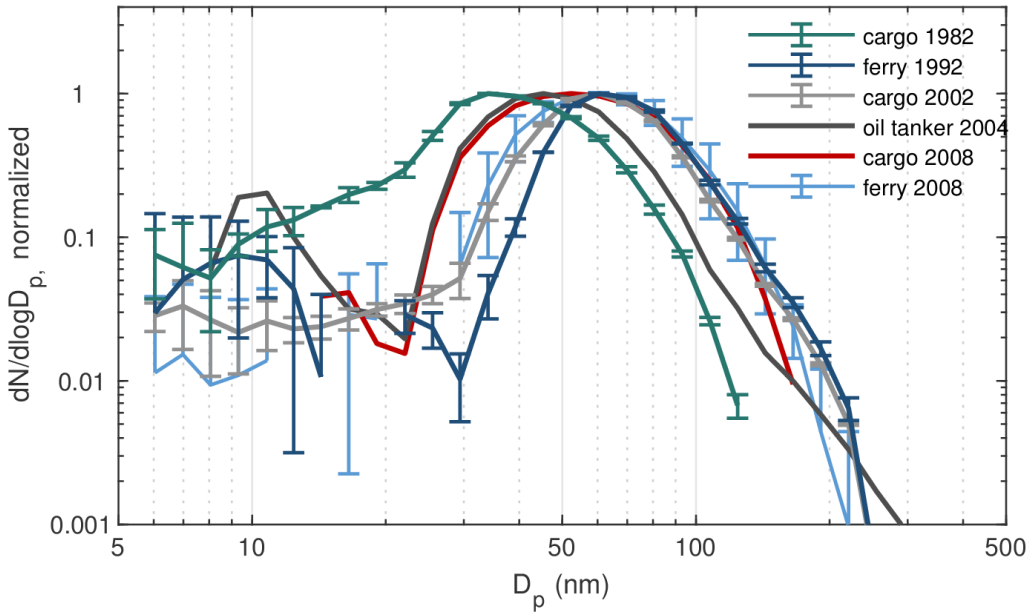

141

142 **Figure S2.** Normalized particle number size distributions measured by EEPS as a mean over in-
143 plume flight for all the ships for which EEPS measurement was available. Error bars denote one
144 standard deviation when multiple chases were conducted.

145

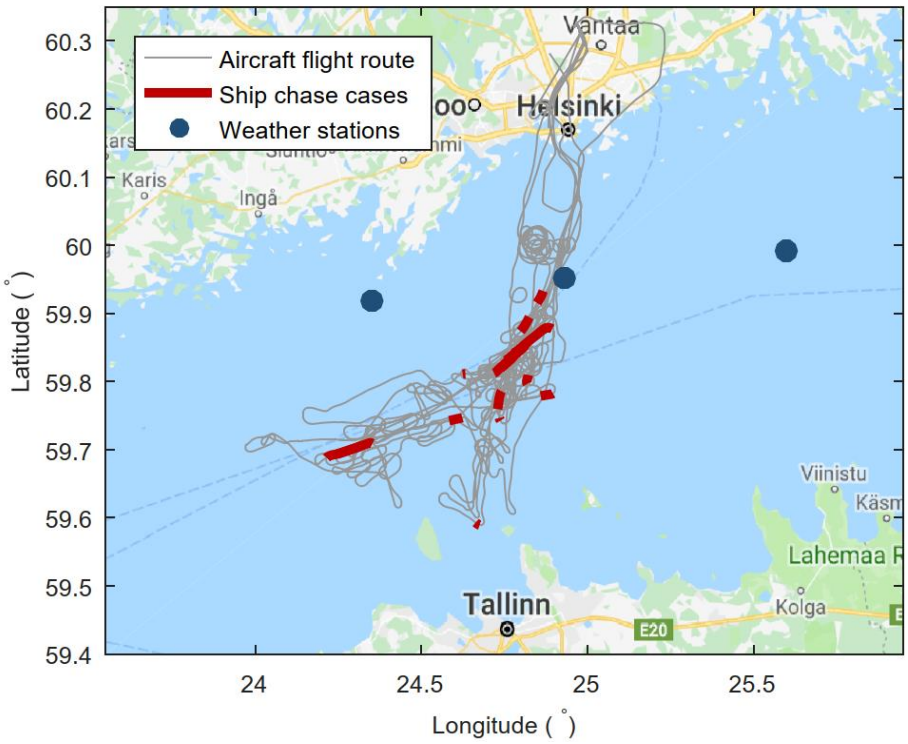

146

147 **Figure S3.** Flight paths of the research aircraft during the chasing measurement of ships
148 operating in the Gulf of Finland.

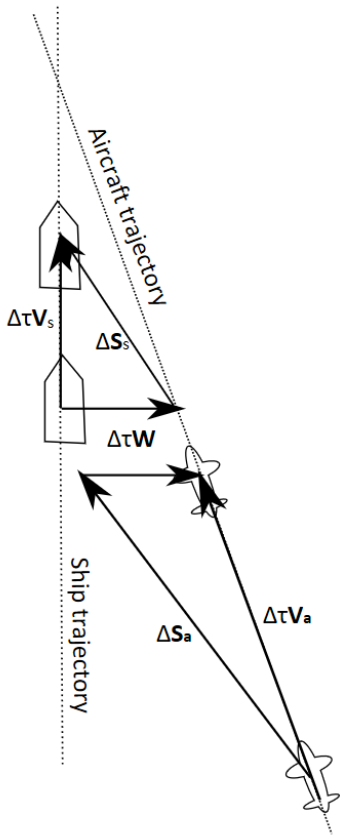

Figure S4. Plot indicating the vectors needed to calculate time correction from the plume sampling time frame to the real atmospheric time frame.

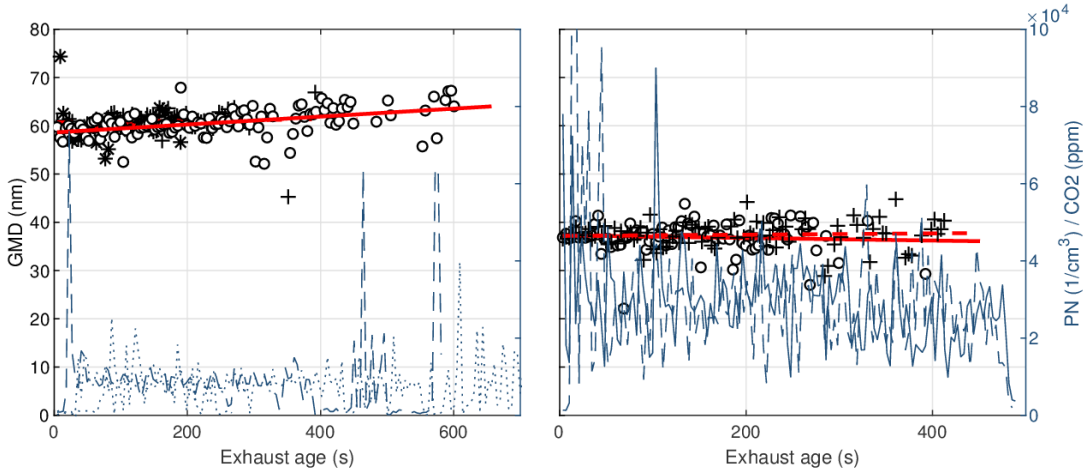

Figure S5. Evolution of geometric mean diameter and PN concentration over two in-plume flights shown in Figure 2. Here particle number concentrations are shown as normalized by CO2 concentration. Varying symbols correspond to separate approaches.

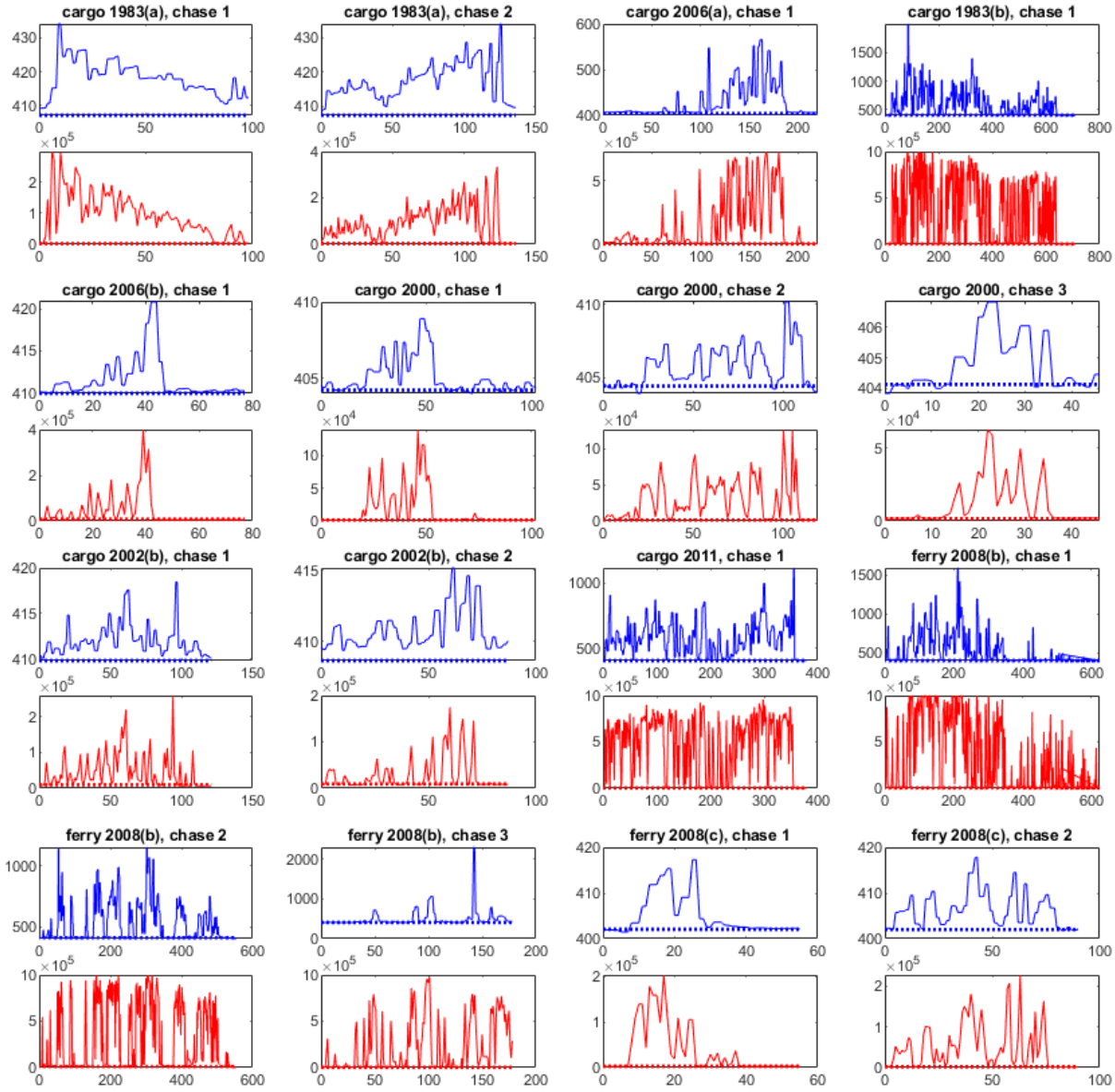

158

159 **Figure S6.** CPC and CO2 analyzer data for the plume chase measurements for the following
160 vessels: cargo 1983(a), cargo 2006(a), cargo 1983(b), cargo 2006(b), cargo 2000, cargo 2002,
161 cargo 2011, ferry 2008(a), and ferry 2008(b). Solid blue lines mark CO_2 concentrations (ppm)
162 during the approaches and dotted blue lines mark the average background CO_2 concentrations
163 (ppm). Analogously, solid red lines mark PN concentrations ($1/cm^3$) during the approaches and
164 dotted red lines mark the average background PN concentrations ($1/cm^3$). All concentrations are
165 plotted against elapsed time (s).

166
167

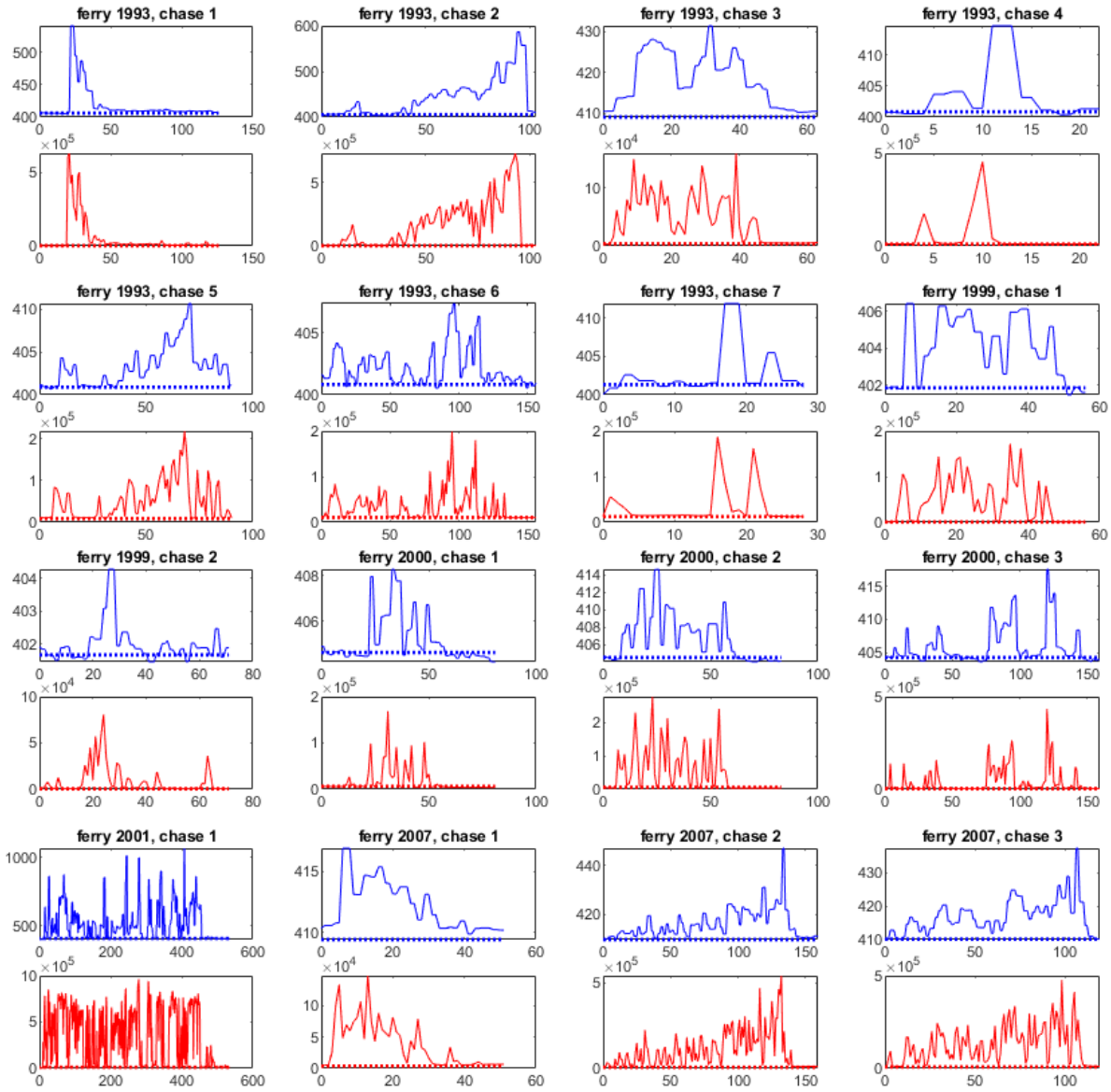

Figure S7. CPC and CO2 analyzer data for the plume chase measurements for the following vessels: ferry 1993, ferry 1999, ferry 2000, ferry 2001, and ferry 2007. Solid blue lines mark CO_2 concentrations (ppm) during the approaches and dotted blue lines mark the average background CO_2 concentrations (ppm). Analogously, solid red lines mark PN concentrations ($1/cm^3$) during the approaches and dotted red lines mark the average background PN concentrations ($1/cm^3$). All concentrations are plotted against elapsed time (s).

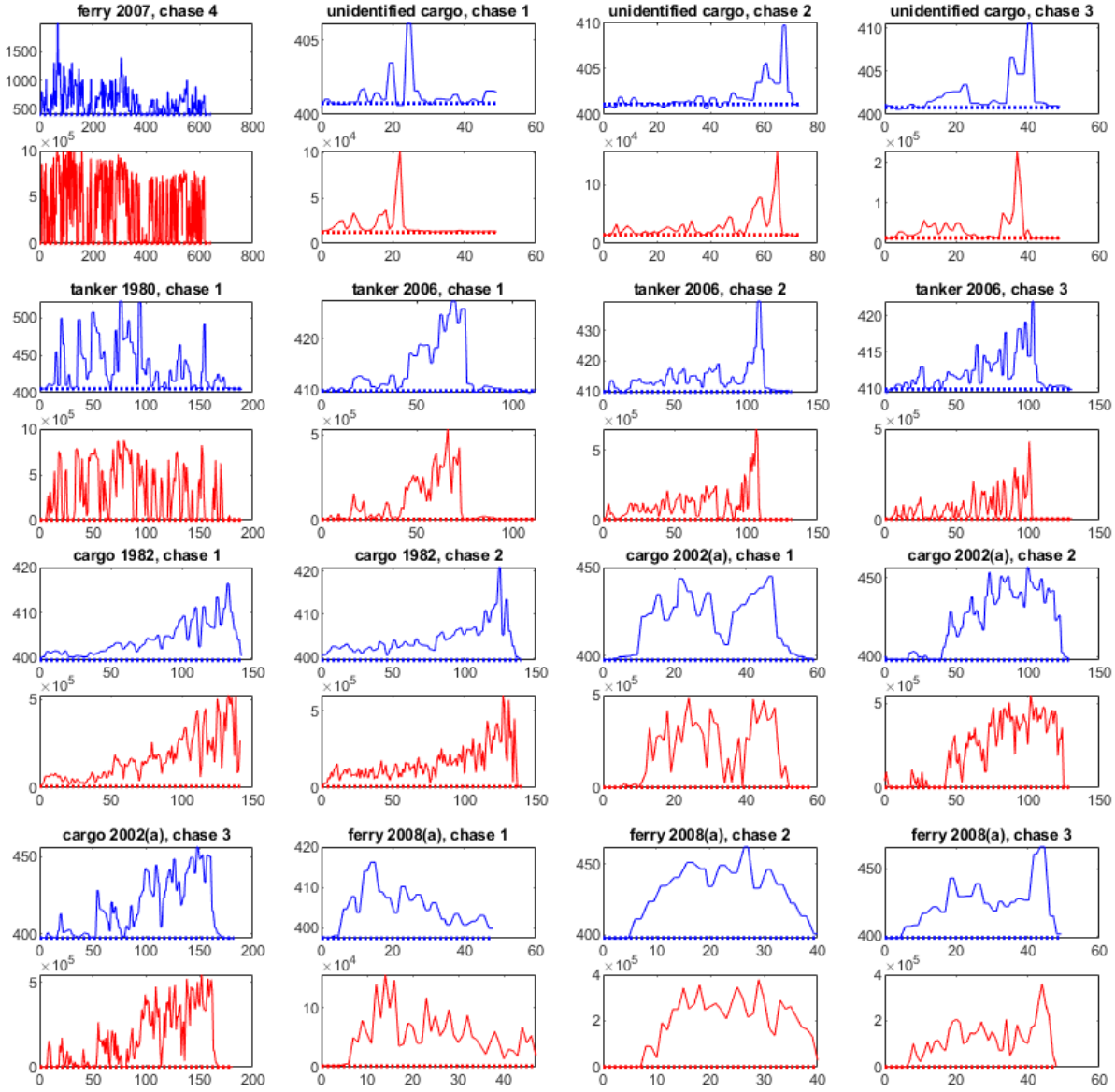

177

178 **Figure S8.** CPC and CO2 analyzer data for the plume chase measurements for the following
179 vessels: ferry 2007, unidentified cargo, tanker 1980, tanker 2006, cargo 1982, cargo 2002, and
180 ferry 2008. Solid blue lines mark CO_2 concentrations (ppm) during the approaches and dotted
181 blue lines mark the average background CO_2 concentrations (ppm). Analogously, solid red lines
182 mark PN concentrations ($1/cm^3$) during the approaches and dotted red lines mark the average
183 background PN concentrations ($1/cm^3$). All concentrations are plotted against elapsed time (s).

184

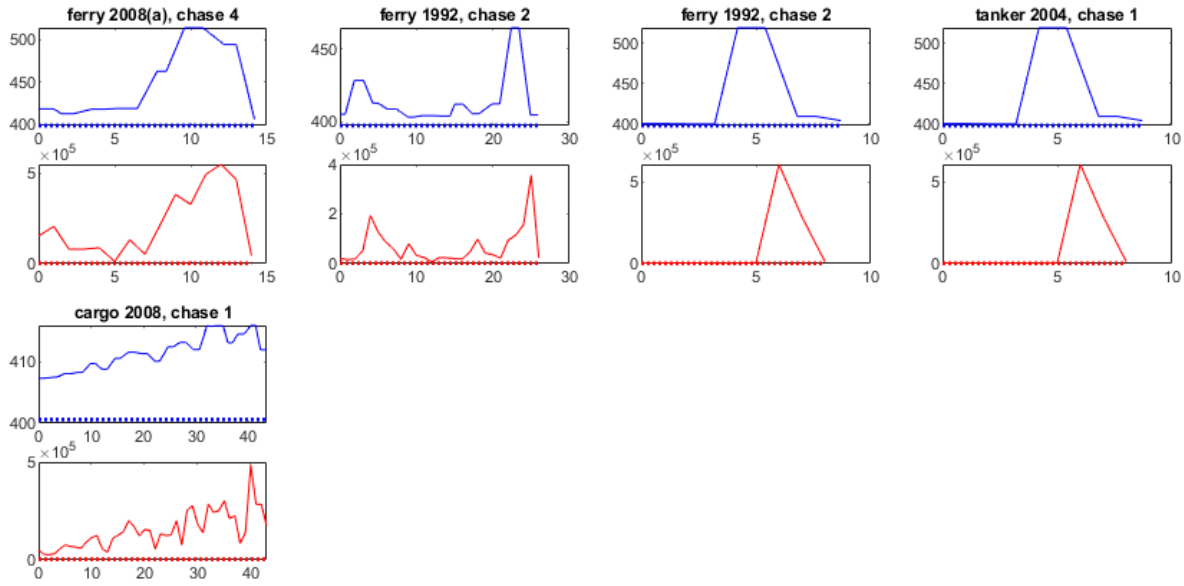

Figure S9. CPC and CO2 analyzer data for the plume chase measurements for the following vessels: ferry 2008, ferry 1992, tanker 2004, and cargo 2008. Solid blue lines mark CO_2 concentrations (ppm) during the approaches and dotted blue lines mark the average background CO_2 concentrations (ppm). Analogously, solid red lines mark PN concentrations (1/cm^3) during the approaches and dotted red lines mark the average background PN concentrations (1/cm^3). All concentrations are plotted against elapsed time (s).

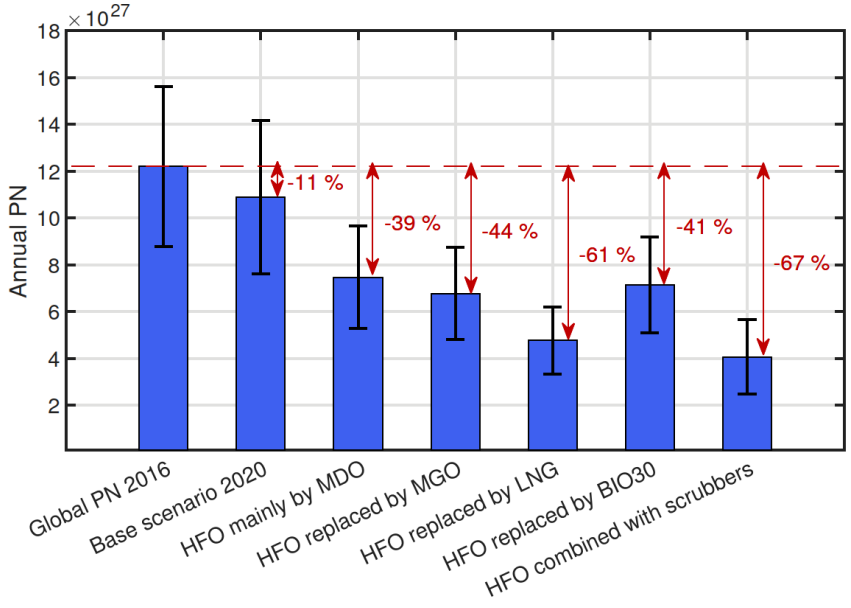

Figure S10. Global annual PN from shipping in 2016 and 2020, as well as the resulting PN from extreme scenarios, where HFO would be mainly replaced by other fuel options than IFO. Error bars denote the combined uncertainty in the estimates. The red annotations mark potential reductions in PN achieved by the presented scenarios.

Table S1. Details of the test-bed engine used during laboratory testing.

Wärtsilä Vasa 4R32 LN E	Liquid fuel operation mode	Natural gas operation mode*
Nominal power (kW)	1640	1400
Number of cylinders	4	4
Speed (rpm)	750	750
Bore (mm)	320	320
Stroke (mm)	350	350
Compression ratio	13.8	12
Rotating direction	clockwise	clockwise
Firing order	1-3-4-2	1-3-4-2
Exhaust valve opens / closes	56° bbdc / 44° atdc	34,8° bbdc / 7,1° atdc
Inlet valve opens / closes	52° btdc / 28° bbdc	9,1° btdc / 35,3° bbdc
Mechanical injection system	Pump L'Orange PEO-GO52, valve L'Orange VUO-U156, nozzle Wärtsilä part number 009422407	Pump L'Orange PEO-GO52, valve L'Orange VUO-G259b, nozzle VUO-U9121b/E / PAAE010974
Static injection advance	12.3°	1: 16.5°, 2: 17.0°, 3: 17.0°, 4: 17.0°
Turbocharger	BBC VTR 254	ABB TPS52-F33 HT 481009

* The modification of the engine to NG operation included, for instance, installing gas admission valves on the cylinder heads, replacing cylinder heads as well as liners, pistons, camshaft and turbocharger. In addition, engine control system was updated and a pilot fuel line with a high pressure pilot fuel pump was added. Exhaust gas piping to stack was equipped with burst disk for safety.

Table S2. Properties of the fuels used in the laboratory and on-board measurements.

Fuel parameter	MGO *	MDO	IFO	HFO 2.2%S	BIO30	HFO 0.7%S
Density (kg/m^3)	838 / 835 (15 ° C)	879 (15 ° C)	906 (40 ° C)	979 (40 ° C)	866 (40 ° C)	873 (15 ° C)
Viscosity (mm^2/s)	3.3 / 2.6 (40 ° C)	4.1 (40 ° C)	127 (50 ° C)	187 (80 ° C)	6.7 (40 ° C)	886 (40 ° C)
Sulphur (mg/kg)	6.3 / 5.9	822	3 750	22 200	< 5	6520
Carbon (wt-%)	86.1 / 86.2	87.4	87.2	85.5	83.5	87.7
Hydrogen (wt-%)	13.9 / 13.8	13.9	12.6	10.3	13.2	11.5
Oxygen (wt-%)	< 0.5 / 0.5	< 0.5	< 0.5	0.5	3.9	0.6
Nitrogen (mg/kg)	19.3 / 61.8	367	2 275	5408	28.5	2490
Ash (wt-%)	< 0.005	< 0.005	0.038 (775 ° C)	0.094 (775 ° C)	< 0.005	<0.005 (775 ° C)
Heating value, lower (kJ/kg)	42.7 / 42.9	42.2	42.1	40.3	40.7	40.8

* MGO was also used as the pilot fuel in MDO and NG measurements, two batches of fuel were tested

Table S3. Particle number emission factors used in the calculations. Standard deviations are shown in parentheses.

Fuel	Cruising		Maneuvering		Weighted average	
	EF_{PN} (#/kg_{fuel})	EF_{PN} (#/kWh)	EF_{PN} (#/kg_{fuel})	EF_{PN} (#/kWh)	EF_{PN} (#/kg_{fuel})	EF_{PN} (#/kWh)
NG*	1.38×10^{16} ($\pm 2.36 \times 10^{15}$)	2.35×10^{15} ($\pm 4.03 \times 10^{14}$)	2.11×10^{16} ($\pm 1.34 \times 10^{15}$)	4.29×10^{15} ($\pm 2.72 \times 10^{14}$)	1.60×10^{16}	2.93×10^{15}
MGO	2.37×10^{16} ($\pm 2.04 \times 10^{15}$)	4.81×10^{15} ($\pm 4.13 \times 10^{14}$)	3.26×10^{16} ($\pm 1.63 \times 10^{15}$)	7.32×10^{15} ($\pm 3.67 \times 10^{14}$)	2.64×10^{16}	5.34×10^{15}
MDO	2.83×10^{16} ($\pm 2.92 \times 10^{15}$)	5.76×10^{15} ($\pm 5.95 \times 10^{14}$)	3.23×10^{16} ($\pm 2.60 \times 10^{15}$)	7.11×10^{15} ($\pm 5.72 \times 10^{14}$)	2.95×10^{16}	6.17×10^{15}
IFO	4.37×10^{16} ($7.29 \pm \times 10^{15}$)	8.88×10^{15} ($\pm 1.48 \times 10^{15}$)	5.69×10^{16} ($\pm 2.50 \times 10^{15}$)	1.36×10^{16} ($\pm 5.99 \times 10^{14}$)	4.76×10^{16}	1.03×10^{16}
HFO 2.2%S	5.39×10^{16} ($\pm 2.77 \times 10^{15}$)	1.16×10^{16} ($\pm 5.94 \times 10^{14}$)	5.83×10^{16} ($\pm 9.42 \times 10^{14}$)	1.47×10^{16} ($\pm 2.37 \times 10^{15}$)	5.52×10^{16}	1.26×10^{16}
BIO30	2.28×10^{16} ($\pm 1.24 \times 10^{15}$)	4.73×10^{15} ($\pm 2.58 \times 10^{14}$)	3.44×10^{16} ($\pm 1.02 \times 10^{15}$)	8.24×10^{15} ($\pm 2.44 \times 10^{14}$)	2.63×10^{16}	5.78×10^{15}
HFO 0.7% S, Engine A						
Before scrubber	3.20×10^{16} ($\pm 1.08 \times 10^{15}$)	6.28×10^{15} ($\pm 2.12 \times 10^{14}$)	4.24×10^{16} ($\pm 6.78 \times 10^{14}$)	8.47×10^{15} ($\pm 1.35 \times 10^{14}$)	3.52×10^{16}	6.93×10^{15}
After scrubber	2.73×10^{15} ($\pm 5.77 \times 10^{13}$)	5.36×10^{14} ($\pm 1.13 \times 10^{13}$)	4.28×10^{15} ($\pm 4.27 \times 10^{14}$)	8.53×10^{14} ($\pm 8.51 \times 10^{13}$)	3.20×10^{15}	6.31×10^{14}
HFO 0.7%S, Engine B						
Before scrubber	2.50×10^{16} ($\pm 1.05 \times 10^{15}$)	4.83×10^{15} ($\pm 2.02 \times 10^{14}$)	3.20×10^{16} ($\pm 9.32 \times 10^{14}$)	6.51×10^{15} ($\pm 1.89 \times 10^{14}$)	2.71×10^{16}	5.33×10^{15}
After scrubber	7.72×10^{15} ($\pm 5.02 \times 10^{14}$)	1.49×10^{15} ($\pm 9.70 \times 10^{13}$)	n/a	n/a	n/a	n/a

*NG burned in dual-fuel operation with MGO as pilot fuel

Table S4. Fuel sulphur content (FSC) and engine after-treatment information for ships involved in the chase study. Fuel sulphur content and exhaust after-treatment data has been provided by the ship operators for part of the vessels. Standard deviation is given in parentheses.

Vessel	EF_{PN} ($1/kg_{fuel}$)	Number of chases	Fuel	FSC (wt%)	Exhaust after-treatment	Classification
cargo 1982	5.8×10^{16} ($\pm 4.9 \times 10^{15}$)	3	HFO	0.99	none	Container Ship
ferry 1992	5.6×10^{15}	2	HFO	0.5	none	Ro-Ro/Passenger Ship
cargo 2002(a)	1.5×10^{16}	2	HFO	0.97	none	Ro-Ro Cargo
tanker 2004	2.3×10^{16}	1	n/a	n/a	n/a	Oil Products Tanker
cargo 2008	6.9×10^{15}	1	HFO	0.94	none	Container Ship
ferry 2008(a)	9.0×10^{15} ($\pm 1.7 \times 10^{15}$)	4	HFO	1	none	Ro-Ro/Passenger Ship
ferry 2008(b)	4.2×10^{15} ($\pm 6.0 \times 10^{13}$)	3	IFO	0.87	none	Ro-Ro/Passenger Ship
ferry 2001	5.0×10^{15}	1	n/a	n/a	n/a	Ro-Ro/Passenger Ship
ferry 2007	2.0×10^{16} ($\pm 1.0 \times 10^{16}$)	4	HFO	1	none	Passenger Ship
cargo 2006(a)	9.6×10^{15}	1	n/a	n/a	n/a	Container Ship
tanker 1980	1.8×10^{16}	1	n/a	n/a	n/a	Oil/Chemical Tanker
cargo 2011	4.7×10^{15}	1	HFO	0.97	none	Ro-Ro Cargo
ferry 1993	1.9×10^{16} ($\pm 1.0 \times 10^{16}$)	7	HFO	1	SCR	Ro-Ro/Passenger Ship
cargo 1983(a)	1.5×10^{16}	2	n/a	n/a	n/a	Container Ship
tanker 2006	3.9×10^{16} ($\pm 1.6 \times 10^{15}$)	3	n/a	n/a	n/a	Crude Oil Tanker
cargo 2006(b)	3.4×10^{16}	1	n/a	n/a	n/a	Container Ship
cargo 2002(b)	2.1×10^{16}	2	n/a	n/a	n/a	Container Ship
unidentified cargo	2.5×10^{16} ($\pm 3.3 \times 10^{15}$)	3	n/a	n/a	n/a	n/a
ferry 2000	3.5×10^{16} ($\pm 1.7 \times 10^{15}$)	3	HFO	0.97	none	Ro-Ro/Passenger Ship
ferry 2008(c)	1.9×10^{16}	2	HFO	0.5	none	Ro-Ro/Passenger Ship
ferry 1999	4.1×10^{16}	2	HFO	0.97	none	Ro-Ro/Passenger
cargo 1983(b)	2.9×10^{15}	1	n/a	n/a	n/a	Reefer
cargo 2000	3.0×10^{16} ($\pm 3.4 \times 10^{15}$)	3	n/a	n/a	n/a	General Cargo

Fuel, fuel sulfur content (FSC), and exhaust after-treatment information has been provided by the shipping companies for part of the ships. Ships are labeled according to their classification in Marine Traffic database (https://marinetraffic.com). During the measurements, FSC in Baltic Sea SECA was limited to 1.0% S.

Table S5. Marine fuel consumption during 2016 and comparison to previous studies.

Fuel	Annual consumption (million tons)[a]	Contribution to total (%)	Consumption with inland contribution (million tons)	IEA, 2011	STEAM, 2015	GHG3, 2012
Residual (HFO)	185	72.1	188	191	195	
Diesel (MDO)	44	17.1	48	62[b]	81[b]	
Gasoil (MGO)	23	9.0	27			
LNG	5	1.9	5			
Total	257		267	254	276	300

[a] Excluding rivers, lakes
[b] Sum of MDO, MGO and LNG

Table S6. Global marine fuel consumptions (Mt) used in calculations for the year 2020.

Fuel consumptions (Mt)	LNG	MGO	MDO	HFO + scrubber	IFO	BIO30
Base scenario 2020	8.20	24.5	46.8	10.9	180	2.73
HFO mainly replaced by MDO	8.20	24.5	2.24	10.9	0	2.73
HFO mainly replaced by MGO	8.20	202	4.68	10.9	0	2.73
HFO mainly replaced by LNG	161	24.5	4.68	10.9	0	2.73
HFO mainly replaced by BIO30	8.20	24.5	4.68	10.9	0	189
HFO mainly replaced by scrubbers	8.20	24.5	4.68	199	0	2.73

Table S7. Summary of methods applied in different parts of the study.

Study	Method	Short description	Reference
Laboratory and on-board tests	Dilution of the sample	Primary dilution: PTD + residence time tube + ejector dilution to mimic ambient dilution conditions Secondary dilution: Ejector diluters and bridge type diluters	(1, 36-38) (39)
	Particle number concentration	Airmodus A20 Condensation Particle Counter, cut-point 7nm	
	Particle number size distribution	SMPS: DMA 3071A and CPC 3775, TSI Inc., size range 10-414 nm; nano-SMPS: DMA 3085 and CPC 3776, TSI Inc., size range 3-64 nm	
	CO_2 concentration	SIDOR Sick Maihak gas analyzer	
	Calculation of PN emission factors	Calculation based on measured engine power, fuel consumption, as well as exhaust mass flow calculated based on the carbon balance method. Wet exhaust gas density approximated according to ISO 8178.	
Ship plume measurements	Sample intake	Skyvan aircraft: BMI Isokinetic Inlet System (Model 1200, Brechtel Manufacturing Inc., USA); two lighter aircrafts: air intake tube with OD of 10 mm and length of 2 m	
	Particle number concentration	Skyvan aircraft: TSI Inc. 3010 Condensation Particle Counter, cut-point 10nm; two lighter aircrafts: TSI Inc. 3776 Condensation Particle Counter, cut-point 3 nm	
	Particle number size distribution	Skyvan aircraft: TSI Inc. Engine Exhaust Particle Sizer, size range 5.6-560 nm (default inversion algorithm)	(41)
	CO_2 concentration	Picarro G1301-m	(40)

	Calculation of PN emission factors	PN emission rate calculation based on time integrals of CPC and CO_2 analyzer signal peaks. Emission factor calculation based on PN emission rate and emission factor of 3.107 kg/kgfuel for CO_2.	(42 eq. 1) (42 eq. 2b, 43)
	Aircraft position, speed, and flight height	GPS recording	
	Ship position and speed	GPS recording	
	Wind speed and direction	Average of three nearby weather stations at Helsinki (Helsingin majakka), Porvoo (Kalbådagrund) and Kirkkonummi Mäkiluoto Corresponding wind data at the aircraft flight height calculated using the power-law wind velocity profile method and assumption of neutral atmospheric conditions.	(SI Ref. 2)
	Plume age	Method analogous to general Doppler effect described in the SI	SI, (SI Ref. 1)
Modelling global PN from ship traffic	Calculating global fuel consumption by fuel type and spatial distribution of PN emissions	STEAM Ship Traffic Emission Assessment Model (Version 3)	(44-47)
	Ship positions and speeds	Global Automatic Identification System (AIS) data, Orbcomm	
	Technical descriptions of ships	IHS Markit database	
	Calculation of fuel usage	Method based on water resistance calculated based on AIS data, separately for main and auxiliary engines Hollenbach water resistance method has been described in Jalkanen et al. (2012) and references within. In short, the method involves the evaluation of wet surface area of the hull, propulsion efficiency determination, hull form calculations and Reynolds/Froude number determination. ITTC friction formula is applied.	(45, and references within)
	Mitigating incomplete AIS data	Smart routing method was used to fill in gaps in AIS. This interpolation routine applied for vessel location determination considers potential land masses between the known two locations.	(47, Appendix B)
	Designation of vessel specific fuel type	Designation based on technical description of engine characteristics and vessel position (following SECA restrictions)	
	Determining specific fuel oil consumption (SFOC) for an engine	Method assuming parabolic dependency of SFOC as function of engine load, operating on the engine manufacturer data of SFOC for each engine	(48)
	Considering effect of scrubbers on SFOC	Method applying 3% additional power consumption for ships with open-loop scrubbers	SI, (SI Ref. 3)
	Considering uncertainty of the global fuel consumption results	Comparisons to vessel fuel reports (Jalkanen et al. 2009, Jalkanen et al. 2012) as well as comparisons to EU MRV reporting scheme.	(44,45)
	Determining share of different fuel options in 2020	Estimates as share of global fuel usage were derived from industry reports.	(49,50)

218

219